JACS
JOURNAL OF THE AMERICAN CHEMICAL SOCIETY
pubs.acs.org/JACS
Article

Parasitic Ferromagnetism in Few-Layered Transition-Metal Chalcogenophosphate

Wei Bai,[#] Zhongqiang Hu,[#] Chong Xiao,* Junqing Guo, Zhou Li, Youming Zou, Xuguang Liu, Jiyin Zhao, Wei Tong, Wensheng Yan, Zhe Qu, Bangjiao Ye, and Yi Xie*

Cite This: *J. Am. Chem. Soc.* 2020, 142, 10849−10855

ABSTRACT: Since the rise of two-dimensional (2D) semiconductors, it seems that electronic devices will soon be upgraded with spintronics, in which the manipulation of spin degree of freedom endows it obvious advantages over conventional charge-based electronics. However, as the most crucial prerequisite for the above-mentioned expectation, 2D semiconductors with adjustable magnetic interaction are still rare, which has greatly hampered the promotion of spintronics. Recently, transition metal phosphates have attracted tremendous interest due to their intrinsic antiferromagnetism and potential applications in spintronics. In the work described herein, parasitic ferromagnetism is achieved for the first time by exfoliating an antiferromagnetic chalcogenophosphate to a few layers. Taking the transition metal chalcogenophosphate $Mn_2P_2S_6$ as an example, the antiferromagnetic transition at the Néel temperature is completely suppressed, and the magnetic behaviors of the as-obtained few-layered $Mn_2P_2S_6$ are dominated by parasitic ferromagnetism. We experimentally verify an electron redistribution by which part of the Mn 3d electrons migrate and redistribute on P atoms in few-layered $Mn_2P_2S_6$ due to the introduced Mn vacancies. The results demonstrated here broaden the tunability of the material's magnetic properties and open up a new strategy to rationally design the magnetic behaviors of 2D semiconductors, which could accelerate the applications of spintronics.

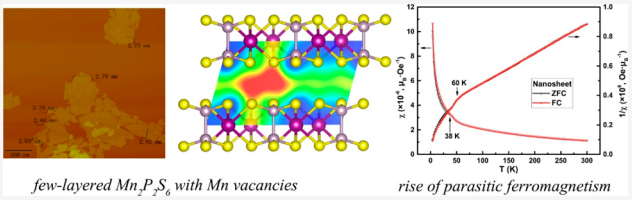

few-layered $Mn_2P_2S_6$ with Mn vacancies *rise of parasitic ferromagnetism*

INTRODUCTION

Spintronics, which exploits the spin degrees of freedom of electrons and thus promises to revolutionize electrical and computer engineering, has generated great interest worldwide because of its long-held prospect for commercial applications in the fields of information storage and logic devices with obvious advantages over conventional charge-based electronics, such as in precise addressing, low energy consumption, and non-volatility.[1,2] However, the limited number of available materials that provide suitable spin transport channels with long spin lifetimes and long-distance spin propagation for various device components presents clear challenges for the above-mentioned purposes.

Since the discovery of graphene, a single atomic layer of graphitic carbon which has promising spin channels with long spin diffusion lengths, intensive research efforts have been devoted to developing spintronics on such a two-dimensional (2D) system.[3] However, it is tricky to open a suitable electronic band gap, and this makes graphene less desirable for the manipulation of charge, which has limited its utilization in circuitry and thus has spawned extensive research on other 2D materials capable of both spin and charge manipulation. Therefore, 2D magnetic semiconductors have received a lot of attention in the past decade, because they not only can be easily obtained by exfoliation due to their weak van der Waals interactions but also incorporate the advantages of both magnetism and semiconductors. Consequently, it is naturally believed that 2D magnetic semiconductors should be the most promising spintronic materials.

The modulation of magnetism in 2D semiconductor materials is a prerequisite for exploring novel phenomena and developing electrically coupled spintronic devices. Even though 2D magnetic semiconductors have been predicted and realized in past research,[4,5] and some approaches have been proposed to tune the magnetic behaviors of 2D semiconductors, such as magnetic doping and proximity effect, there is still obviously a lack of sufficient candidates and a general tuning approach for spintronic applications. The key reason is that most of the 2D semiconductors are naturally antiferromagnetic and tend to show very weak responses to ordinary external field; the lack of large-scale synthesis methods also restricts their widespread applications.

Received: April 15, 2020
Published: May 20, 2020

https://dx.doi.org/10.1021/jacs.0c04101
J. Am. Chem. Soc. 2020, 142, 10849−10855

Herein, we obtain parasitic ferromagnetism for the first time in exfoliated van der Waals antiferromagnetic semiconductors. Taking chalcogenophosphate as an example, the magnetic behavior of few-layered $Mn_2P_2S_6$ changes significantly such that the antiferromagnetic transition at the Néel temperature in susceptibility measurements is completely suppressed and the magnetic behaviors are dominated by parasitic ferromagnetism. Mn vacancies are introduced during the exfoliation process, as demonstrated by positron annihilation spectroscopy. The consequent electron redistribution, by which part of the Mn 3d electrons migrate and redistribute on P atoms after exfoliation, is verified by near-edge X-ray absorption fine structure spectroscopy and shown to be the origin of the parasitic ferromagnetism in few-layered $Mn_2P_2S_6$. The results reported here broaden the tunability of the material's magnetic properties and elucidate a new strategy and direction for rational design of 2D magnetic semiconductors.

EXPERIMENTAL SECTION

Synthesis of $Mn_2P_2S_6$. Single crystals of $Mn_2P_2S_6$ were grown by chemical vapor transport without a halogen transport agent, avoiding the introduction of halogen impurities. A mixture of stoichiometric Mn, P, and S powder was evacuated and sealed into a quartz tube. The hot zone of the furnace used was 750 °C, and the temperature gradient was 100 °C. Pieces of transparent green plates up to 3 × 3 mm^2 were obtained at the cold zone. Few-layered $Mn_2P_2S_6$ was synthesized by an ion-exchange exfoliation process.[6,7] The crystals obtained in this way were stirred in 2 M KCl aqueous solution, followed by centrifugation and decantation. The precipitate was dispersed in 3 M LiCl·H_2O aqueous solution and continually stirred for 3 h. The precipitate was collected and dispersed in a 5% aqueous solution of polyvinylpyrrolidone (PVP). The dispersion was ultrasonicated for 2 h and left standing overnight. The supernatant was centrifuged, washed several times with a water−ethanol mixture, and dried in N_2 at 60 °C.

Characterization of Lattice Structure and Morphology. X-ray diffraction (XRD) characterization was done on a Philips X'Pert Pro Super X-ray diffractometer with Cu Kα (λ = 1.5418 Å) radiation. The morphology and selected-area electron diffraction (SAED) pattern were observed with a JEM-2100F field emission electron microscope; charge accumulation may destroy the lattice structure, which requires decreasing the irradiation time when the electron diffraction is analyzed. The thickness of the flakes was measured in tapping mode using a DI MultiMode V scanning probe microscope.

Characterization of Positron Annihilation Spectra. The positron lifetime experiments were carried out by a fast−slow coincidence ORTEC system with a time resolution of about 230 ps full width at half-maximum. The lifetime and the density distribution of a positron in a perfect bulk crystal or of a positron trapped at a defect were calculated by solving the three-dimensional Kohn−Sham equation with the finite difference method based on the conventional scheme and density functional theory.

Characterization of Magnetic Properties. Magnetic properties were measured by using a magnetic property measurement system (MPMS). Bulk single-crystal $Mn_2P_2S_6$ and few-layered $Mn_2P_2S_6$ powder after drying were used for magnetic measurements. The temperature was varied from 4 to 300 K, and the maximum magnetic field was up to 7 T.

Characterization by Near-Edge X-ray Absorption Fine Structure (NEXAFS), Raman Spectroscopy, and Electron Spin Resonance (ESR). The samples for NEXAFS measurement were affixed on 3M copper foil tape and measured at the National Synchrotron Radiation Laboratory (NSRL). The Raman signals were recorded under pump vacuum using a T64000 Horiba spectrometer with copper foil as substrate. A Bruker EMXplus spectrometer was used to measure the ESR signal by sweeping the field between 0 and 8000 G at a microwave frequency of 9.409 GHz.

RESULTS AND DISCUSSION

The 2D van der Waals semiconductor $Mn_2P_2S_6$ is a layered transition metal chalcogenophosphate with the structural motif $M_2P_2X_6$ (M = transition metals, X = S, Se), of which the unit cell belongs to monoclinic $C2/m$ (space group 12). Mn^{2+} ions are surrounded by distorted chalcogen octahedra and linked with $[P_2X_6]^{4-}$ bipyramids, forming 2D planes (Figure 1a). In each monolayer, the magnetic moment on Mn^{2+} atoms aligns perpendicularly to the *ab* plane and constitutes a honeycomb lattice (Figure 1b). Although the detailed magnetic[8−12] and optical properties[13−16] resulting from interlayer coupling are still illusive and under studies, $Mn_2P_2S_6$ is generally described with the 2D Heisenberg model in which the moments on neighboring manganese atoms in the same layer are coupled antiferromagnetically.

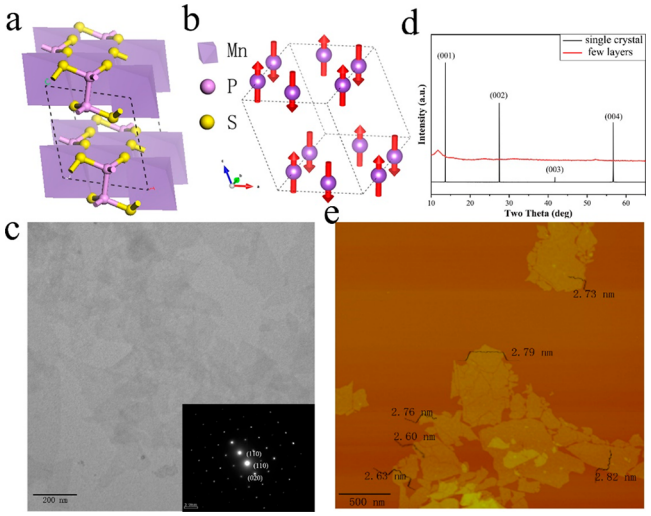

Figure 1. Crystal structure of $Mn_2P_2S_6$. (a) Mn^{2+} ions are represented by distorted octahedra to indicate that they are surrounded by sulfur atoms. Mn^{2+} is linked by $[P_2S_6]^{4-}$ groups (shown as ball-and-stick model), forming a 2D layer. (b) Magnetic lattice structure of Mn^{2+} ions. Only Mn^{2+} ions are presented. (c) Transmission electron microscopy (TEM) image of few-layered $Mn_2P_2S_6$ and selected-area electron diffraction (SAED) pattern. (d) X-ray diffraction (XRD) patterns of single-crystal and few-layered $Mn_2P_2S_6$. (e) Atomic force microscopy (AFM) images of few-layered $Mn_2P_2S_6$.

In this study, few-layered $Mn_2P_2S_6$ was successfully synthesized by liquid exfoliation. The transmission electron microscopy (TEM) image and the electron diffraction along the electron incidence direction [001] of few-layered $Mn_2P_2S_6$ are presented in Figure 1c. After exfoliation, the interplanar spacing of (110) and (1−10) shrink by ∼5.7% and ∼7.9% separately and the interplanar spacing of (020) shrinks by ∼4.3% compared with their bulk counterparts, which means that exfoliation applies shrinkage stress on the crystal lattice and intensifies the distortion of the Mn−S octahedron in few-layered $Mn_2P_2S_6$. Figure 1d illustrates the XRD patterns of single-crystal and exfoliated few-layer samples, respectively. Only (00*l*) diffraction can be clearly observed in the crystal sample, indicating the layered structure with a period of 6.51 Å and also confirming the high purity of the as-grown crystals. As to few-layered $Mn_2P_2S_6$, only one broad diffraction at d = 7.55 Å is observed, which could be assigned to the (001) facet due to the preferred orientation caused by layer-by-layer assembly during XRD measurement. The high-angle shift of (001)

https://dx.doi.org/10.1021/jacs.0c04101
J. Am. Chem. Soc. 2020, 142, 10849−10855

compared with the bulk counterparts indicates the increase of interplanar spacing by about 16%, which derives from the destruction of the van der Waals gap. Atomic force microscopy (AFM) (Figure 1e) and the corresponding height distribution show the non-overlapped flakes averaging 2.5−3 nm thickness, deduced to be 3−4 layers according to the (001) interplanar spacing obtained from the maximum peak d = 7.55 Å in Figure 1d.

During the exfoliation process, Mn vacancies are introduced according to the elemental analysis (Figure 2a). In order to get

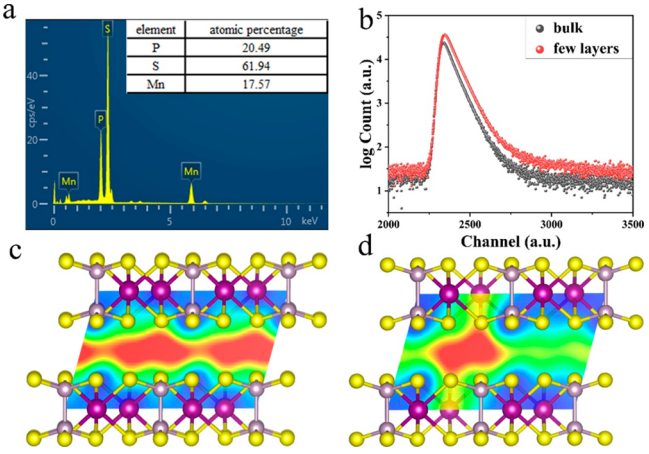

Figure 2. Mn vacancies in $Mn_2P_2S_6$. (a) Elemental analysis by energy-dispersive X-ray spectra. (b) Positron annihilation spectrometry of bulk and few-layered samples. Schematic representation of trapped positrons for (c) pure crystal lattice and (d) Mn vacancies. The section is parallel to the *bc* plane and cuts through a Mn vacancy.

an in-depth analysis of this non-stoichiometry, positron annihilation spectrometry (PAS), which is a non-destructive and selective means of detecting negatively charged centers in a material, was employed to study the type and relative concentration of Mn vacancies in the bulk and few-layered $Mn_2P_2S_6$. Through β+ decay, the radioisotope ^{22}Na emits positrons that diffuse randomly and annihilate with the electrons in the tested sample. By measuring the intensity of photons emitted after annihilation and fitting it with an exponential equation, the mean lifetimes of the positrons are obtained, which can provide inside information about the type and concentration of defects in the material (Figure 2b). Basically speaking, there is a background lifetime when positrons annihilate in a perfect lattice, and any additional negative electron center will trap the positrons and lead to a longer annihilation process. In total, three types of positron annihilation processes are found in our measurements (Table 1). In bulk $Mn_2P_2S_6$, only τ_1 = 296 ps and τ_3 = 717 ps exist, which are associated with the free annihilation in the pure crystal lattice (on the order of hundreds of picoseconds) and the annihilation in the van der Waals gap (on the order of nanoseconds), respectively[17] (Figure 2c). However, for few-layered $Mn_2P_2S_6$, we can only get a satisfactory result by fitting

Table 1. Positron Lifetime Parameters of Bulk and Few-Layered $Mn_2P_2S_6$

	τ_1 (ps)	τ_2 (ps)	τ_3 (ps)	I_1 (%)	I_2 (%)	I_3 (%)
bulk	296	–	717	94.7	–	5.3
few layers	306	465	1880	86.2	12.4	1.4

three instead of two positron annihilation processes. The additional τ_2 = 465 ps represents a longer lifetime of positrons compared with τ_1. Therefore, the lifetime of this trapping state is longer than that in the pure crystal lattice, and we identify it as the contribution of Mn vacancies (Figure 2d). It is also to be noted that τ_3 = 1880 ps is much longer than that in bulk sample, which demonstrates the rise of a more loosely stacked structure compared with the van der Waals structure after exfoliation. The changes of positron lifetimes in the few-layered sample clearly demonstrate the break of the van der Waals gap and the existence of Mn vacancies.

For van der Waals magnetic materials, the interlayer coupling is considered to be relatively weak,[18] while the Mn vacancies greatly affect the honeycomb magnetic structure of $Mn_2P_2S_6$ and lead to significant changes in the magnetic behavior of few-layered $Mn_2P_2S_6$. The magnetic properties of single-crystal and few-layered $Mn_2P_2S_6$ are measured by a MPMS. It is to be noted that single-crystal $Mn_2P_2S_6$ shows anisotropy when the applied magnetic field is perpendicular to or parallel to the *ab* plane ($\chi_\perp$ and $\chi_\parallel$). From Figure 3a, both $\chi_\perp$

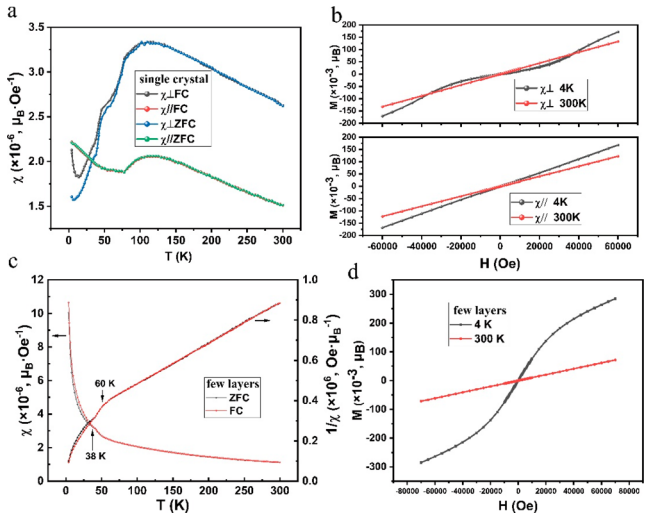

Figure 3. Magnetic properties of $Mn_2P_2S_6$. (a) Temperature dependence of magnetic susceptibility of single-crystal $Mn_2P_2S_6$ under 1000 Oe. (b) The M−H curves of single-crystal $Mn_2P_2S_6$ when applied field is perpendicular to ($\chi_\perp$) or parallel to ($\chi_\parallel$) the *ab* plane. (c) Temperature dependence of magnetic susceptibility of exfoliated few-layered $Mn_2P_2S_6$ under 1000 Oe. (d) The M−H curves of few-layered $Mn_2P_2S_6$.

and $\chi_\parallel$ show a broad antiferromagnetic transition peak around 105 K. The broad range of transition temperature is due to short-range spin−spin correlation.[19] Below 105 K, both $\chi_\perp$ and $\chi_\parallel$ decrease with decreasing temperature, which indicates the formation of antiferromagnetic order. When the temperature reaches 78 K, $\chi_\perp$ and $\chi_\parallel$ start to show a different tendency, in which $\chi_\perp$ still decreases but $\chi_\parallel$ starts to slightly increase with decreasing temperature. Therefore, 78 K is identified as the Néel temperature (T_N). Overall, the behaviors of $\chi_\perp$ and $\chi_\parallel$ agree well with the mean field approximation (MFA) model except for three points. First, $\chi_\perp$ and $\chi_\parallel$ above T_N are not equal. However, we can attribute this to the difference of background for each measurement, because the difference between $\chi_\perp$ and $\chi_\parallel$ nearly keeps constant with varying temperature above T_N. Second, when the decreasing temperature reaches 6 K, $\chi_\perp$ (both field-cooled (FC) and zero-field-cooled (ZFC) data)

https://dx.doi.org/10.1021/jacs.0c04101
J. Am. Chem. Soc. 2020, 142, 10849−10855

starts to increase instead of continuously decreasing, which results from the paramagnetic impurities.[20] Third, $\chi_{\parallel}$ slightly increases instead of keeping constant below T_N, which is attributed to the onset of long-range antiferromagnetic order arising from a combination of dipole−dipole anisotropy with interplanar coupling.[21−24] Figure 3b shows the $M-H$ data for perpendicular and parallel measurements. At 300 K, both of the $M-H$ lines are linear. When the temperature is 4 K, however, the $M-H$ line for the perpendicular measurement is inverse S-shaped, while that for the parallel measurement is still linear. The reason is proposed to be a spin-flop transition.[25] When the applied field is along the spin orientation (perpendicular to the *ab* plane), it will be parallel to one of the spin moments and antiparallel to another. When the applied field is above a critical value, the spin moment that is antiparallel to it will flop, in order to achieve the minimization of the energy. In this spin-flop state, the two spin moments will form an angle and the orientation of the applied field is exactly the bisector of this angle. This transition will lead to a jump of magnetization at such a critical magnetic field. The spin-flop transition field is approximately 20 kOe in $Mn_2P_2S_6$. All of the above proofs demonstrate that the spins of $Mn_2P_2S_6$ bulk are basically in an antiferromagnetic arrangement.

After being exfoliated to a few layers, the magnetic behavior of $Mn_2P_2S_6$ changes a lot compared with that of the bulk counterpart. From Figure 3c, the $1/\chi-T$ curve of few-layered $Mn_2P_2S_6$ above 60 K obeys the Curie−Weiss law, with a Weiss constant of $\theta = -147$ K. The negative θ value suggests that the antiferromagnetic coupling among Mn^{2+} ions still dominates in few-layered $Mn_2P_2S_6$, even though the anticipated broad transition around 105 K is totally suppressed. Instead, an apparent transition appears at 38 K, where the FC and ZFC curves both start to increase rapidly with the decreasing temperature but branch away from each other, which is a sign of weak ferromagnetism. We propose that this transition arises from spin canting, which tends to align the adjacent Mn^{2+} spins off-antiparallel to each other but non-collinear antiferromagnetic coupling with a small angle and forming a perturbation state, leading to non-zero magnetization and a weak ferromagnetic interaction. Usually, the canting of spin moments is caused by either magnetocrystalline anisotropy or Dzyaloshinsky−Moriya antisymmetric interaction.[26−28] In our case, the factor is assumed to be the latter one for the following two reasons. One is that all the Mn atoms are located in distorted octahedra, having similar chemical environments and acting with a collective spin behavior according to our ESR measurement (Figure 4). Because of the exchange interactions in bulk $Mn_2P_2S_6$, 3d electrons on Mn(II) lose their isolated paramagnetic property and exhibit a collective behavior which

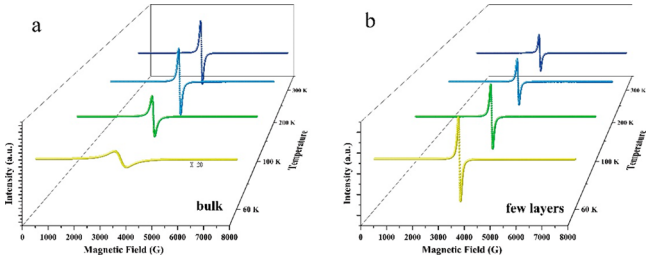

Figure 4. Electron spin resonance (ESR) spectra of $Mn_2P_2S_6$. ESR absorption of (a) bulk and (b) few-layered $Mn_2P_2S_6$ at 60, 100, 200, and 300 K. Microwave frequency: 9.409 GHz.

leads to a single-line ESR spectrum without hyperfine structure,[29] demonstrating the existence of spin exchange interactions. The other is because of the rise of Mn vacancies, the inversion symmetry of magnetic lattice is broken, which leads to a non-zero Dzyaloshinsky−Moriya interaction. The divergence of FC and ZFC curves in Figure 3c also indicates the history dependence of the magnetization process, thereby demonstrating the existence of such a spin-canting-caused weak ferromagnetic state, which at the macroscopic level is called parasitic ferromagnetism. Different from bulk $M-H$ curves (inverse S-shape for perpendicular measurement and linear for parallel measurement), Figure 3d shows an S-shaped $M-H$ curve in a few-layered sample at 4 K, which is exactly another important feature of a weak ferromagnetic state. The absence of an obvious hysteresis loop is a characteristic of a soft magnet. To sum up, the few-layered $Mn_2P_2S_6$ shows parasitic ferromagnetism, by which the basic antiferromagnetic interaction is parasitized by a weak ferromagnetism.

The rise of parasitic ferromagnetism in few-layered $Mn_2P_2S_6$ can be explained by the Mn vacancies introduced during the exfoliation process; the electron configuration on Mn atoms is crucial to exchange interactions and determines their magnetic properties. In order to explain the effect of Mn vacancies on magnetism, the interband electron transitions of bulk and few-layered $Mn_2P_2S_6$ were studied by NEXAFS measurements. An energy-adjustable synchrotron extreme UV source is used to irradiate the sample, and the absorption intensity is measured. The intensity of L-edge absorption is positively correlated to the probability of a transition from 2p electrons to unoccupied states.[30] As for $Mn_2P_2S_6$, the unoccupied states are composed of Mn 3d, P 3p, and S 3p orbitals.[31,32] After exfoliation, Mn L-edge absorption increases (Figure 5a), which means a higher

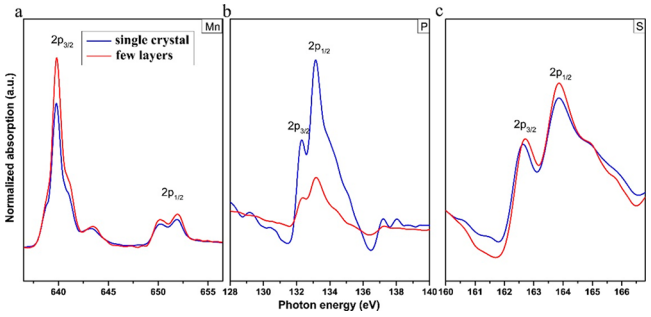

Figure 5. Near-edge X-ray absorption fine structure (NEXAFS) measurements for L-edge (a) Mn, (b) P, and (c) S. Blue and red curves represent single-crystal and few-layered $Mn_2P_2S_6$, respectively.

probability of transition and a larger density of unoccupied Mn 3d states in the few-layered sample than in the bulk. These redundant 3d electrons, generated from Mn vacancies, have to migrate and redistribute in order to maintain electric neutrality. As clearly indicated by Figure 5b,c, the absorption of the P L-edge decreases and the S L-edge keeps almost unchanged, which means the redundant 3d electrons prefer to localize on P's 3p orbital and fill part of P's 3p empty states. The redistribution of electrons lowers the electron density on Mn ions, destroys part of the antiferromagnetic exchange interactions, and thereby leads to the perturbation state which is regarded as the origin of parasitic ferromagnetism.

The electron redistribution also affects the polarization of chemical bonds in $Mn_2P_2S_6$, which is characterized by Raman spectroscopy. The few-layered $Mn_2P_2S_6$ for Raman measure-

https://dx.doi.org/10.1021/jacs.0c04101
J. Am. Chem. Soc. 2020, 142, 10849−10855

ments is prepared by dropping and naturally drying the ethanol dispersion on copper foil. Ordinary Raman (Figure 6a) and

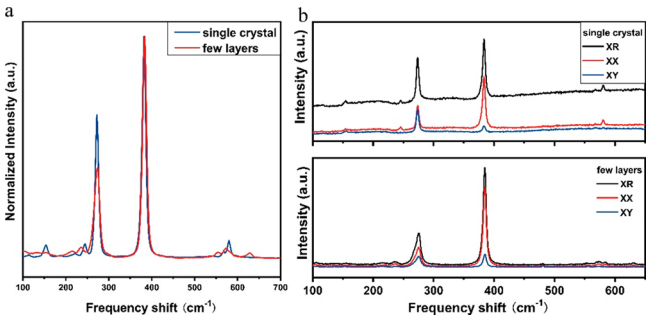

Figure 6. (a) Ordinary and (b) polarized Raman spectroscopy of single-crystal and few-layered $Mn_2P_2S_6$. For ordinary Raman, the intensity is normalized by a peak at ~381 cm^{-1}, while for polarized Raman, the intensity is untreated and radiation time is 100, 50, and 50 s for XR, XX, and XY modes, respectively.

polarized Raman (Figure 6b) spectroscopy is carried out at room temperature. XX and XY represent that the analyzer is parallel to or perpendicular to the laser polarization axis, respectively. XR represents the mode without the polarization analyzer. If the depolarization ratio $\rho = I(XY)/I(XX) < 0.75$, the vibration is polarized and arises from a totally symmetric vibrational mode. If $\rho = 0.75$, it is depolarized and arises from a non-symmetric mode.[33] The characteristics of several major vibrations are listed in Table 2. Some vibration modes redshift

Table 2. Raman Frequency Shift (cm^{-1}), Vibration Mode, and Symmetry of Several Major Vibrations Extracted from Figure 6[a]

single crystal	154	222	244	272	381	567	580
few layers	132	214	235	274	383	553	572
vibration mode	E_g	E_g	A_g	E_g	A_g	E_g	A_g
polarized (p)/ depolarized (dp)	dp	dp	p	dp	p	dp	p

[a]The representation and polarization types are determined by our experiments and ref 35.

after exfoliation (such as 222, 244, 567, and 580 cm^{-1}), which cannot be explained simply as phonon softening caused by nanocrystallization,[34] because other peaks keep the same wavenumber after exfoliation (such as 272 and 384 cm^{-1}, which are identified by the metal-cation motion and overall vibration of the $[P_2S_6]^{4-}$ group[35]). Basically, the vibrations of bonds change the polarizability of the electric dipole and increase the Raman signal. The polarizability is a description of the deformability of the electron cloud under monochromatic light (electric field). The redshift of Raman modes indicates that less energy is needed for exciting this kind of deformability, and the increased polarizability is attributed to the additional mobility of electrons of Mn−P and P−S bonds caused by the electron redistribution.

Based on the above experiments and analyses, we propose an interpretation of the parasitic ferromagnetism in few-layered $Mn_2P_2S_6$. In $Mn_2P_2S_6$, the magnetic moments are primarily localized on Mn^{2+} and coupled antiferromagnetically by the dominated nearest-neighbor direct exchange interaction and superexchange interaction.[10] After exfoliation, vacancies and stress are introduced, and the Mn 3d electrons migrate and redistribute on P atoms, which weakens the antiferromagnetic exchange interaction and forms a non-collinear spin-canting state which is the mechanism of parasitic ferromagnetism.

CONCLUSION

In summary, we highlight an unexpected acquisition of parasitic ferromagnetism in few-layered transition-metal chalcogenophosphate $Mn_2P_2S_6$ from its antiferromagnetic bulk counterpart for the first time. Mn vacancies are introduced during the exfoliation process, which is clearly confirmed by positron annihilation spectra. Manifested by NEXAFS and Raman spectra, the redistribution of Mn 3d electrons triggered by such Mn vacancies is discovered, which leads to the unexpected parasitic ferromagnetism after exfoliation by lowering the electron density on Mn ions and affecting the polarization of the chemical bonds. As a result, in few-layered $Mn_2P_2S_6$ the anticipated antiferromagnetic transition at the Néel temperature around 78 K is suppressed; instead, an apparent transition appears at 38 K, where the FC and ZFC curves both increase with the decreasing temperature but branch away from each other while the $M-H$ line becomes S-shaped, which provides indisputable evidence of parasitic ferromagnetism. The newly discovered parasitic ferromagnetism in few-layered transition-metal chalcogenophosphate from its antiferromagnetic bulk counterpart not only provides a generic understanding of magnetic behaviors of 2D semiconductors but also elucidates a new strategy and direction of rational design of 2D magnetic semiconductors. The modulation of magnetism in 2D semiconductors is especially critical to integrated logic and storage devices such as spin transistors/diodes because of their abilities to transport electrons and spin at the same time. We envision that the demonstrated parasitic ferromagnetism in few-layered semiconductor $Mn_2P_2S_6$ will open up new possibilities for applications of spintronics.

AUTHOR INFORMATION

Corresponding Authors

Chong Xiao − *Hefei National Laboratory for Physical Sciences at the Microscale, CAS Center for Excellence in Nanoscience, University of Science and Technology of China, Hefei, Anhui 230026, P. R. China; Institute of Energy, Hefei Comprehensive National Science Center, Hefei, Anhui 230031, P. R. China;* orcid.org/0000-0002-6134-6086; Email: cxiao@ustc.edu.cn

Yi Xie − *Hefei National Laboratory for Physical Sciences at the Microscale, CAS Center for Excellence in Nanoscience, University of Science and Technology of China, Hefei, Anhui 230026, P. R. China; Institute of Energy, Hefei Comprehensive National Science Center, Hefei, Anhui 230031, P. R. China;* orcid.org/0000-0002-1416-5557; Email: yxie@ustc.edu.cn

Authors

Wei Bai − *Hefei National Laboratory for Physical Sciences at the Microscale, CAS Center for Excellence in Nanoscience, University of Science and Technology of China, Hefei, Anhui 230026, P. R. China*

Zhongqiang Hu − *Hefei National Laboratory for Physical Sciences at the Microscale, CAS Center for Excellence in Nanoscience, University of Science and Technology of China, Hefei, Anhui 230026, P. R. China*

https://dx.doi.org/10.1021/jacs.0c04101
J. Am. Chem. Soc. 2020, 142, 10849−10855

Junqing Guo − *State Key Laboratory of Particle Detection and Electronics, University of Science and Technology of China, Hefei, Anhui 230026, P. R. China*

Zhou Li − *Hefei National Laboratory for Physical Sciences at the Microscale, CAS Center for Excellence in Nanoscience, University of Science and Technology of China, Hefei, Anhui 230026, P. R. China;* orcid.org/0000-0002-6355-0291

Youming Zou − *High Magnetic Field Laboratory (HMFL), Hefei Institutes of Physical Science, CAS, Hefei, Anhui 230031, P. R. China*

Xuguang Liu − *Hefei National Laboratory for Physical Sciences at the Microscale, CAS Center for Excellence in Nanoscience, University of Science and Technology of China, Hefei, Anhui 230026, P. R. China*

Jiyin Zhao − *Hefei National Laboratory for Physical Sciences at the Microscale, CAS Center for Excellence in Nanoscience, University of Science and Technology of China, Hefei, Anhui 230026, P. R. China*

Wei Tong − *High Magnetic Field Laboratory (HMFL), Hefei Institutes of Physical Science, CAS, Hefei, Anhui 230031, P. R. China*

Wensheng Yan − *National Synchrotron Radiation Laboratory, University of Science and Technology of China, Hefei, Anhui 230029, P. R. China;* orcid.org/0000-0001-6297-4589

Zhe Qu − *High Magnetic Field Laboratory (HMFL), Hefei Institutes of Physical Science, CAS, Hefei, Anhui 230031, P. R. China*

Bangjiao Ye − *State Key Laboratory of Particle Detection and Electronics, University of Science and Technology of China, Hefei, Anhui 230026, P. R. China*

Complete contact information is available at: https://pubs.acs.org/10.1021/jacs.0c04101

Author Contributions

#W.B. and Z.H. contributed equally.

Notes

The authors declare no competing financial interest.

■ ACKNOWLEDGMENTS

This work was financially supported by the National Key R&D Program of China (2018YFB0703602, 2017YFA0303500, 2019YFA0210000), the National Natural Science Foundation of China (21622107, U1832142, and 21805269), the Youth Innovation Promotion Association CAS (2016392), the Fundamental Research Funds for the Central University (WK2340000094), the Key Research Program of Frontier Sciences (QYZDY-SSW-SLH011), China Postdoctoral Science Foundation (2019TQ0293), and the National Synchrotron Radiation Laboratory Joint funds of University of Science and Technology of China (KY2340000114).

■ REFERENCES

(1) Awschalom, D. D.; Flatté, M. E. Challenges for semiconductor spintronics. *Nat. Phys.* **2007**, *3*, 153−159.

(2) Fert, A. Nobel Lecture: Origin, development, and future of spintronics. *Rev. Mod. Phys.* **2008**, *80*, 1517.

(3) Han, W.; Kawakami, R. K.; Gmitra, M.; Fabian, J. Graphene spintronics. *Nat. Nanotechnol.* **2014**, *9*, 794.

(4) Gong, C.; Li, L.; Li, Z.; Ji, H.; Stern, A.; Xia, Y.; Cao, T.; Bao, W.; Wang, C.; Wang, Y.; Qiu, Z. Q.; et al. Discovery of intrinsic ferromagnetism in two-dimensional van der Waals crystals. *Nature* **2017**, *546*, 265−269.

(5) Huang, B.; Clark, G.; Navarro-Moratalla, E.; Klein, D. R.; Cheng, R.; Seyler, K. L.; Zhong, D.; Schmidgall, E.; McGuire, M. A.; Cobden, D. H.; Yao, W.; Xiao, D.; Jarillo-Herrero, P.; Xu, X. Layer-dependent ferromagnetism in a van der Waals crystal down to the monolayer limit. *Nature* **2017**, *546*, 270−273.

(6) Frindt, R. F.; Yang, D.; Westreich, P. Exfoliated single molecular layers of $Mn_{0.8}PS_3$ and $Cd_{0.8}PS_3$. *J. Mater. Res.* **2005**, *20*, 1107−1112.

(7) Yang, D.; Westreich, P.; Frindt, R. F. Exfoliated $CdPS_3$ single layers and restacked films. *J. Solid State Chem.* **2002**, *166*, 421−425.

(8) Long, G.; Henck, H.; Gibertini, M.; Dumcenco, D.; Wang, Z.; Taniguchi, T.; Watanabe, K.; Giannini, E.; Morpurgo, A. F. Persistence of magnetism in atomically thin $MnPS_3$ crystals. *Nano Lett.* **2020**, *20*, 2452−2459.

(9) Li, X.; Wu, X.; Yang, J. Half-Metallicity in $MnPSe_3$ Exfoliated Nanosheet with Carrier Doping. *J. Am. Chem. Soc.* **2014**, *136*, 11065−11069.

(10) Sivadas, N.; Daniels, M. W.; Swendsen, R. H.; Okamoto, S.; Xiao, D. Magnetic ground state of semiconducting transition-metal trichalcogenide monolayers. *Phys. Rev. B: Condens. Matter Mater. Phys.* **2015**, *91*, 235425.

(11) Evans, J. S.; O'Hare, D.; Clement, R.; Leaustic, A.; Thuéry, P. Origins of the spontaneous magnetization in $MnPS_3$ intercalates: a magnetic susceptibility and powder neutron diffraction study. *Adv. Mater.* **1995**, *7*, 735−739.

(12) Evans, J. S. O.; O'Hare, D.; Clement, R. The Structure of $Co(\eta\text{-}C_5H_5)^{2+}$ and NMe^{4+} Intercalates of $MnPS_3$: An X-ray, Neutron-Diffraction, and Solid-State NMR Study. *J. Am. Chem. Soc.* **1995**, *117*, 4595−4606.

(13) Du, K. Z.; Wang, X. Z.; Liu, Y.; Hu, P.; Utama, M. I. B.; Gan, C. K.; Xiong, Q. H.; Kloc, C. Weak van der Waals stacking, wide-range band gap, and Raman study on ultrathin layers of metal phosphorus trichalcogenides. *ACS Nano* **2016**, *10*, 1738−1743.

(14) Kuo, C. T.; Neumann, M.; Balamurugan, K.; Park, H. J.; Kang, S.; Shiu, H. W.; Kang, J. H.; Hong, B. H.; Han, M.; Noh, T. W.; Park, J. G. Exfoliation and Raman spectroscopic fingerprint of few-layer $NiPS_3$ van der Waals crystals. *Sci. Rep.* **2016**, *6*, 20904.

(15) Lee, J. U.; Lee, S.; Ryoo, J. H.; Kang, S.; Kim, T. Y.; Kim, P.; Park, C.-H.; Park, J.-G.; Cheong, H. Ising-type magnetic ordering in atomically thin $FePS_3$. *Nano Lett.* **2016**, *16*, 7433−7438.

(16) Susner, M. A.; Chyasnavichyus, M.; Puretzky, A. A.; He, Q.; Conner, B. S.; Ren, Y.; Cullen, D. A.; Ganesh, P.; Shin, D.; Demir, H.; McMurray, J. W.; Borisevich, A. Y.; Maksymovych, P.; McGuire, M. A. Cation−Eutectic Transition via Sublattice Melting in $CuInP_2S_6$/$In_{4/3}P_2S_6$ van der Waals Layered Crystals. *ACS Nano* **2017**, *11*, 7060−7073.

(17) Murakami, H.; Tsutsumi, Y.; Marutani, D.; Sano, M.; Ichimura, K. Formation of Vacancies in Layered MPS_3 (M = Fe, Mn, Zn) upon Intercalation. *Mater. Sci. Forum* **2001**, *363*−*365*, 380−382.

(18) Wildes, A. R.; Roessli, B.; Lebech, B.; Godfrey, K. W. Spin waves and the critical behaviour of the magnetization in $MnPS_3$. *J. Phys.: Condens. Matter* **1998**, *10*, 6417.

(19) Joy, P. A.; Vasudevan, S. Magnetism in the layered transition-metal thiophosphates MPS_3 (M= Mn, Fe, and Ni). *Phys. Rev. B: Condens. Matter Mater. Phys.* **1992**, *46*, 5425.

(20) Long, G.; Zhang, T.; Cai, X.; Hu, J.; Cho, C.-w.; Xu, S.; Shen, J.; Wu, Z.; Han, T.; Lin, J.; Wang, J.; Cai, Y.; Lortz, R.; Mao, Z.; Wang, N.; et al. Isolation and characterization of few-layer manganese thiophosphite. *ACS Nano* **2017**, *11*, 11330−11336.

(21) Kurosawa, K.; Saito, S.; Yamaguchi, Y. Neutron diffraction study on $MnPS_3$ and $FePS_3$. *J. Phys. Soc. Jpn.* **1983**, *52*, 3919−3926.

(22) Ouvrard, G.; Brec, R.; Rouxel, J. Structural determination of some MPS_3 layered phases (M= Mn, Fe, Co, Ni and Cd). *Mater. Res. Bull.* **1985**, *20*, 1181−1189.

(23) Wildes, A. R.; Rønnow, H. M.; Roessli, B.; Harris, M. J.; Godfrey, K. W. Static and dynamic critical properties of the quasi-two-dimensional antiferromagnet $MnPS_3$. *Phys. Rev. B: Condens. Matter Mater. Phys.* **2006**, *74*, 094422.

(24) Ressouche, E.; Loire, M.; Simonet, V.; Ballou, R.; Stunault, A.; Wildes, A. Magnetoelectric $MnPS_3$ as a candidate for ferrotoroidicity. *Phys. Rev. B: Condens. Matter Mater. Phys.* **2010**, *82*, 100408.
(25) Yagotintsev, K. A.; Strzhemechny, M. A.; Prokhvatilov, A. I.; Stetsenko, Y. E.; Vysochanskii, Y. M. Interlayer Mn−Mn exchange parameter in $MnPS_3$ from x-ray diffraction data. *Low Temp. Phys.* **2012**, *38*, 383−385.
(26) Manson, J. L.; Kmety, C. R.; Palacio, F.; Epstein, A. J.; Miller, J. S. Low-field remanent magnetization in the weak ferromagnet $Mn[N(CN)_2]_2$. Evidence for spin-flop behavior. *Chem. Mater.* **2001**, *13*, 1068−1073.
(27) Jia, H. P.; Li, W.; Ju, Z. F.; Zhang, J. A two-step field-induced magnetic transition in spin-canted systems observed only for the Co II coordination polymer. *Chem. Commun.* **2008**, *3*, 371−373.
(28) Palacio, F. Inducing Spontaneous Magnetization in Antiferromagnets. *Mol. Cryst. Liq. Cryst. Sci. Technol., Sect. A* **1997**, *305*, 385−399.
(29) Köseoğlu, Y.; Yildiz, F.; Yakhmi, J. V.; Qin, J.; Chen, X.; Aktaş, B. EPR studies on BEDT-TTF intercalated $MnPS_3$ molecular magnet. *J. Magn. Magn. Mater.* **2003**, *258*, 416−418.
(30) Lin, F.; Liu, Y.; Yu, X.; Cheng, L.; Singer, A.; Shpyrko, O. G.; Xin, H. L.; Tamura, N.; Tian, C. X.; Weng, T.-C.; Yang, X.-Q.; Meng, Y. S.; Nordlund, D.; Yang, W. L.; Doeff, M. M. Synchrotron X-ray analytical techniques for studying materials electrochemistry in rechargeable batteries. *Chem. Rev.* **2017**, *117*, 13123−13186.
(31) Sugiura, C.; Kamata, A.; Nakai, S. I. X-Ray Spectroscopic Investigation of the Valence-Band Structure of Layered Compounds MPS_3 (M= Mn, Fe, Ni, Zn, Mg). *J. Phys. Soc. Jpn.* **1996**, *65*, 2152−2157.
(32) Chittari, B. L.; Park, Y.; Lee, D.; Han, M.; MacDonald, A. H.; Hwang, E.; Jung, J. Electronic and magnetic properties of single-layer MPX_3 metal phosphorous trichalcogenides. *Phys. Rev. B: Condens. Matter Mater. Phys.* **2016**, *94*, 184428.
(33) Strommen, D. P. Specific values of the depolarization ratio in Raman spectroscopy: Their origins and significance. *J. Chem. Educ.* **1992**, *69*, 803.
(34) Yang, M.; Huang, D.; Hao, P.; Zhang, F.; Hou, X.; Wang, X. Study of the Raman peak shift and the linewidth of light-emitting porous silicon. *J. Appl. Phys.* **1994**, *75*, 651−653.
(35) Bernasconi, M.; Marra, G. L.; Benedek, G.; Miglio, L.; Jouanne, M.; Julien, C.; Scagliotti, M.; Balkanski, M. Lattice dynamics of layered MPX_3 (M= Mn, Fe, Ni, Zn; X= S, Se) compounds. *Phys. Rev. B: Condens. Matter Mater. Phys.* **1988**, *38*, 12089.

https://dx.doi.org/10.1021/jacs.0c04101
J. Am. Chem. Soc. 2020, 142, 10849−10855